Turbulence effects on phytoplankton morphofunctional traits selection

Stéphane Fraisse,* Myriam Bormans, Yvan Lagadeuc
Université de Rennes 1, UMR CNRS 6553 ECOBIO, Campus de Beaulieu, Rennes cedex, France

Abstract

Turbulence can regulate phytoplankton community structure in aquatic ecosystems by affecting sedimentation and nutrient acquisition. In rivers, nutrient concentrations are often high enough to sustain phytoplankton growth without limitation. Hence, turbulence mainly acts on phytoplankton by controlling its vertical position in such ecosystems. We conducted a laboratory experiment to see if the response of phytoplankton to turbulence could be predicted from morphofunctional traits related to sinking velocity and maximum growth rate. Turbulence was generated by horizontally oscillating grid systems in three 5 L chambers, which also constituted three chemostats. Two turbulence levels typical of lowland rivers ($\varepsilon = 7.9 \times 10^{-5}\,m^2\,s^{-3}$ and $\varepsilon = 7.8 \times 10^{-3}\,m^2\,s^{-3}$) were tested on an experimental community composed of six species from different taxonomic lineages. The species selected displayed different values for five morphofunctional traits related to sinking velocity and maximum growth rate (S : V ratio, algal unit size, density, shape, and motility). We showed that community structure could be partly predicted from morphofunctional traits. Under low turbulence (LT) ($\varepsilon = 7.9 \times 10^{-5}\,m^2\,s^{-3}$), species displaying traits leading to high sinking velocity (i.e., large size and high density) were unable to sustain stable populations, whereas species which displayed the opposite traits (i.e., small size, flattened shape, or low density) dominated the community. Furthermore, one of the six species exhibited phenotypic plasticity in size and could adapt to both high and LT conditions.

Functional traits, first investigated in plants, are increasingly used to understand phytoplankton community structure in response to environmental factors (Litchman and Klausmeier 2008; Kruk et al. 2011; Fraisse et al. 2013). A functional trait can be defined as any physiological and/or morphological feature at the individual level which provides a competitive advantage in a given environment (McGill et al. 2006; Violle et al. 2007). Morphological traits are of particular interest as they are easily measurable and constitute good proxies for physiological traits (Weithoff 2003; Kruk et al. 2010). Initially described as "life-forms" by Margalef (1978), they are currently widely known as morphofunctional traits. In phytoplankton, one of the most obvious morphofunctional traits is cell size. This is related to physiological traits controlling nutrient acquisition such as μ_{max} (maximum growth rate), V_{max} (maximum uptake rate) and K_s (half saturation constant), resulting in a competitive advantage for small species in a nutrient-limited environment (Aksnes and Egge 1991; Edwards et al. 2012; Marañón et al. 2013). Size, given its range of variation in phytoplankton, has often been considered as a master trait. However, phytoplankton can exhibit numerous morphofunctional traits. For instance, shape affects diffusive transport, thus impacting nutrients acquisition, and results in competitive advantages for elongated as compared to spherical cells (Pahlow et al. 1997). The presence of flagella can also influence nutrient uptake, allowing cells to reach layers of higher nutrient concentration (Gervais 1997; Pithart 1997). This is a decisive advantage in aquatic ecosystems where sedimentation may often be the major process of phytoplankton loss. Hence, other traits controlling sinking velocities such as shape (Padisák et al. 2003), and the faculty to reduce density (Walsby 1994; Reynolds 2007) directly impact phytoplankton fitness. The importance of these traits is dependent on the turbulence level of a given ecosystem.

Indeed, in aquatic systems, turbulence is the dominant physical process controlling the distribution of dissolved and particulate matter (Thorpe 2007) and is assumed to be the most important factor (with nutrient supply) shaping the cell through evolution and "the only reason for proceeding to a functional interpretation of morphology" (Margalef 1978). Turbulence plays a key role in regulating phytoplankton community structure, maintaining negatively buoyant taxa in the water column while homogenizing positively buoyant ones (Bormans and Condie 1998; Huisman et al. 1999; Peeters et al. 2007). Turbulence can also affect phytoplankton growth rate, the laminar shear induced by turbulence increasing the nutrient fluxes to cells below the

*Correspondence: steph.fraisse@gmail.com

ACCEPTED MANUSCRIPT

Table 1. Morphofunctional and functional traits values for the different species, where S : V ratio is the surface to volume ratio, MLD is the maximum linear dimension, Φ is the form coefficient resistance (for elongated form, horizontal, and vertical values, respectively, indicated), ρ' is the density, ESR is the equivalent spherical radius, V_{st} is the theoretical sinking velocity (for elongated form, horizontal, and vertical values are, respectively, indicated), V_{sm} is the measured sinking velocity (under still conditions) and μ_{max} is the maximum growth rate (measured under still conditions. Values in brackets are the standard deviation.

	Elongated shape		Flattened shape		Flagellated cell	
	S. pulchellum	*A. granulata*	*A. formosa*	*P. boryanum*	*C. curvata*	*N. olivacea*
Class	Zygnematophyceae	Bacillariophyceae	Bacillariophyceae	Chlorophyceae	Cryptophyceae	Prasinophyceae
S : V ratio	0.8	1.23	1.20	1	0.3	1.3
Shape	Elongated	Elongated	Flattened	Flattened	Spherical	Spherical
Motility	X	X	X	X	Flagellated	Flagellated
MLD (μm)	184.6 ($\pm$130.6)	80.9 ($\pm$40.5)	28.2 ($\pm$3.9)	18.8 ($\pm$9.5)	31 ($\pm$6.0)	6.2 ($\pm$1.1)
Φ	2.3–1.5	1.45–0.92	5	1.86	X	X
ρ' (kg m^{-3})	1078 $\pm$ 2	1103 $\pm$ 2	1103 $\pm$ 2	1070 $\pm$ 4	1040	1040
ESR (μm)	13.3 ($\pm$3.9)	5.0 ($\pm$1.1)	4.5 ($\pm$2.0)	4.7 ($\pm$1.4)	12.9 ($\pm$8.2)	2.1 ($\pm$0.2)
V_{st} (μm s^{-1})	12.2–18.6	3.8–6.0	0.9	1.8	X	X
V_{sm} (μm s^{-1})	14.4 ($\pm$1.2)	3.2 ($\pm$0.4)	4.2 ($\pm$0.5)	1.1 ($\pm$0.0)	X	X
μ_{max} (day^{-1})	0.12 ($\pm$0.02)	0.50 ($\pm$0.07)	0.42 ($\pm$0.01)	0.18 ($\pm$0.08)	0.10 ($\pm$0.05)	0.17 ($\pm$0.02)

Kolmogorov scale (i.e., scale of the smallest vortices that fluid motion supports in the face of viscosity, *see* Material and methods for calculation; Lazier and Mann 1989; Kiøboe 1993; Karp-Boss et al. 1996). The resulting increase in nutrient fluxes is mostly significant for large species ($>60\,\mu$m; Lazier and Mann 1989; Karp-Boss et al. 1996), as illustrated experimentally by Peters et al. (2006) but may also be significant for smaller species ($20\,\mu$m) due to the intermittency of turbulence (Lagadeuc 2005). Cell organization also matters as filaments experience a greater increase in nutrient fluxes than solitary forms (Pahlow et al. 1997). However, turbulence may have the exact opposite effect and reduce the growth rate through loss of flagella (e.g., Thomas and Gibson 1990), mechanical destruction (e.g., Hondzo and Lyn 1999) or the inhibition of cell division (Berdalet 1992; Sullivan and Swift 2003). Hence, turbulence, through both positive and negative effects, plays a key role in structuring the phytoplankton community (Estrada and Berdalet 1997; Smayda and Reynolds 2001).

Previous studies of the role of turbulence on phytoplankton have mainly focused on marine species and those on freshwater species were often conducted in lakes (Hondzo and Lyn 1999; Hondzo and Warnaars 2008). For instance, Margalef (1978) investigated the functional role of different phytoplankton life-forms and determined which ones were best adapted depending on turbulence. However, large spatio-temporal fluctuations in turbulence can occur in rivers and play a role in shaping the phytoplankton community, especially its vertical distribution (Descy and Gosselain 1994; Reynolds 2000; Tavernini et al. 2011). Different morphofunctional traits related to sedimentation rate may thus be selected depending on the intensity of turbulence (Cózar and Echevarría 2005; Fraisse et al. 2013). However, variations in turbulence level usually co-occur with other environmental factors (like residence time, temperature, nutrient availability), thus highlighting the need for controlled experimental studies where all these confounding factors can be kept constant and the effects of turbulence isolated.

The aim of this study was to determine experimentally if the lotic phytoplankton community structure under contrasted turbulence regimes could be predicted from the morphofunctional traits. Two levels of turbulence were tested in nutrient replete conditions on a simplified phytoplankton community composed of species displaying different morphofunctional traits related to maximum growth rate (μ_{max}) and sinking velocity. We hypothesized that under low turbulence (LT), morphofunctional traits associated with low sinking velocity would be selected. However, if the phytoplankton community was prevented from sinking under high turbulence (HT), it was expected be structured according to morphofunctional traits related to μ_{max}, with leading species displaying higher μ_{max} becoming dominant.

Material and methods

Morphofunctional traits of selected species

The phytoplankton community tested was a simplified one, composed of six species typical of riverine environments. These species were chosen according to morphofunctional traits related to different known sinking velocities and also to different values of μ_{max} (Table 1).

Two species were flagellated (*Nephroselmis olivacea*-CCAP1960/4B and *Cryptomonas curvata*-CCAP979/62) and the four others were organized either in filaments

ACCEPTED MANUSCRIPT

(*Aulacoseira granulata*-CCAP1002/1 and *Spondylosium pulchellum*-CCAP680/1) or flattened colonies (*Pediastrum boryanum*-CCAP261/20 and *Asterionella formosa*-CCAP1005/17). The nonflagellated species were expected to display different sinking velocities, according to their shape, with higher values for elongated shapes. *A. formosa* and *A. granulata* are diatom species, and hence have a higher density (the heaviest diatoms attaining up to 1290 kg m^{-3}) than other species (1040 kg m^{-3}) (Reynolds 2006) which is also reflected in the sinking velocity. The selected species ranged in size from 2 μm to 17.5 μm. In this study, the whole algal unit size (unicellular, filament or colony depending on the species) was considered. As individual species displayed complex forms, size was expressed as the equivalent sphere radius (ESR) which corresponds to the radius of a sphere of equivalent volume. Cell volumes were calculated by measuring at least 20 individual cells of each species in each sample following Hillebrand et al. (1999) [*N. olivacea* and *C. curvata*: prolate spheroid; *A. granulata*: cylinder; *A. formosa*: box + two cylinders; *S. pulchellum*: ellipsoid; and *P. boryanum*: elliptic prism].

Due to the size range of phytoplankton species, the surrounding environment is characterized by a low Reynolds number ($Re < 0.1$) (Naselli-Flores and Barone 2011). Under these viscous conditions, the sinking velocity of inert spherical particles can be estimated from the Stokes equation (Clift et al. 1978). However, the selected species were not of spherical shape. Hence, a modified Stokes equation was used suitably adapted to calculate the sinking velocity V_{st} (m s^{-1}) of particles displaying complex shapes (Jaworski et al. 1988):

$$V_{st} = \frac{2gr^2(\rho' - \rho)}{9\eta\Phi} \quad (1)$$

where g is the gravitational acceleration (9.81 m s^{-2}), r (m) the ESR of the particle and ρ' (kg m^{-3}) its density (Table 1). ρ is the medium density (999.5 kg m^{-3} at 18°C) and η its dynamic viscosity ($\sim 1.002 \times 10^{-3}$ kg $m^{-1} s^{-1}$ at 18°C). ϕ (a dimension-less number) is the form resistance coefficient which is dependent on shape and reflects the factor by which the sinking velocity of the particles differs from that of a sphere of identical volume and density (Jaworski et al. 1988; Padisák et al. 2003; Walsby and Holland 2006).

As phytoplankton species display a wide range of densities, ranging from 1040 up to 1280 kg m^{-3} for diatoms (Reynolds 2006), the sinking velocity was calculated by measuring the density of each species by density gradient centrifugation, as described by Walsby and Holland (2006). Percoll (Sigma) in 10 mL tubes was subjected to ultracentrifugation ($\sim 30{,}000 \times g$ for 40 min) to obtain a linear density gradient, ranging from 1000 kg m^{-3} at the top to 1150 kg m^{-3} at the bottom of the tube. The phytoplankton suspension was then layered over this gradient and another series of centrifugations was run ($\sim 530 \times g$ at the middle of the tube for 20 min). The sample migrated from the top to the isodensity layer, forming a green band (for *S. pulchellum* and *P. boryanum*) or a light brown band (for *A. formosa* and *A. granulata*). The phytoplankton band was then removed with a glass Pasteur pipette and its refractive-index was measured. The density was calculated from the refractive-index/density calibration curve obtained from measurements on a series of 10 dilutions of Percoll. The physical integrity of each species was assessed microscopically after the $530 \times g$ centrifugation (at 400X magnification) and no cell deterioration was observed.

The form resistance coefficient was derived empirically for each species and set of experimental conditions. For *P. boryanum* and *A. formosa*, we used the value inferred by Padisák et al. (2003), which depends on the number of cells in the colony. For phytoplankton of elongated shape (*S. pulchellum* and *A. granulata*), ϕ depends on their orientation in relation to the direction of movement (McNown and Malaika 1950):

$$\phi = \frac{16}{3D\ (\alpha + \beta)} \quad (2)$$

We, therefore, calculated ϕ for vertical and horizontal positions. In this equation, β is a shape factor depending on the sinking orientation (for details, *see* Walsby and Holland 2006). Two theoretical boundary velocities, corresponding to vertical and horizontal positions, were calculated.

The sinking velocity (V_{sm}) of each species was measured in still water following Smith (1982).

$$C_t = C_0\left(1 - \frac{V_{sm}\ t}{z}\right) \quad (3)$$

where C_t (cells mL^{-1}) is the phytoplankton concentration in the water column at time t (s), C_0 (cells mL^{-1}) is the phytoplankton concentration at $t = 0$ (uniform with depth), V_{sm} is the sinking velocity (m s^{-1}) and z is the height of the Utermöhl chamber. An inverted microscope and Utermöhl device were used to count the live phytoplankton cells appearing at the bottom of the chamber at regular time intervals (five minutes), in a view centered in the middle of the column to minimize wall effects, and the time t_x at which $C_t = 0$ (when no further variation was observed in the number of cells counted at the bottom of the chamber) was estimated. Hence, Eq. 3 becomes:

$$V_{sm} = \frac{z}{t_x} \quad (4)$$

from which we can calculate V_{sm}. Although it cannot be excluded that a thermal convection might have occurred during our measurements, which could have greatly influenced the sinking velocity of each species, we took great care to minimize such a phenomenon inside the chamber. Hence, during determination of the appearance rate, the laboratory temperature was set at the same value used for algal maintenance and for the experiments (i.e., 18°C). Furthermore, we conducted our measures in a small chamber column (height = 0.0095 m; diameter = 0.026 m) as the

ACCEPTED MANUSCRIPT

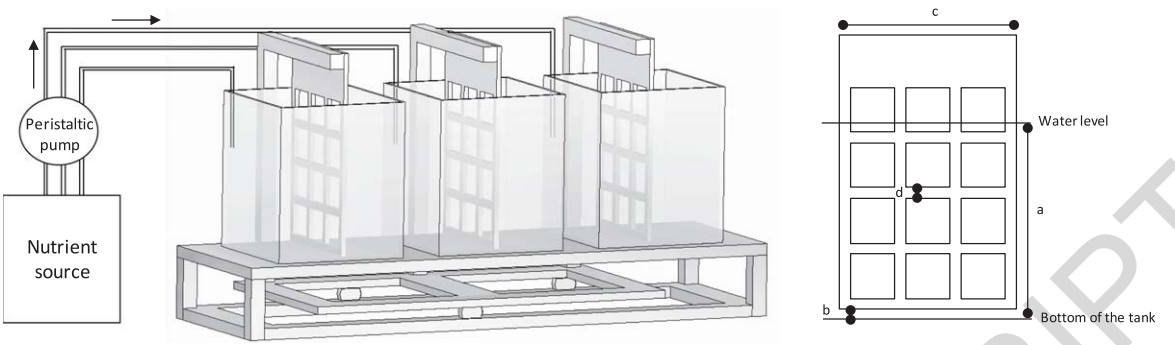

Fig. 1. The turbulence generating device is composed of three grids, each fixed on an arm connected to a moving frame. The translation motion of this moving frame is controlled by an electric motor (not shown) and results in horizontal oscillation of the grids. The velocity of grid oscillation depends on the electric voltage intensity supplied to the motor. Hence, the same turbulence intensity is generated in each tank, which includes three replicates. Each tank also constitutes a chemostat, as new medium is constantly supplied through a peristaltic pump. The same volume is also removed (tubes not shown) to keep the total volume constant (4.9 L). A dilution rate of 0.07 per day was applied. The grid is represented at the right of the figure. 1.65×10^{-1} m of it (code a) was under water as it was placed 5×10^{-3} m (code b) above the bottom of the tank, corresponding to a total immersed area immerged equal to 2.64×10^{-2} m^2 (length = 1.65×10^{-1} m, width = 1.6×10^{-1} m, code c). Each hole (4×10^{-2} m square) is separated by 1×10^{-2} m from the next one, and from the edge (code d).

likelihood of convection currents occurring is greater in columns with a large height/diameter ratio (>5) (Hötzel and Croome 1999). The Utermöhl chamber was kept under the microscope throughout the settling measurements.

The selected species displayed different surface to volume ratios (S : V ratio), calculated following Hillebrand et al. (1999), a trait known to be related to maximum growth rate (Banse 1976). They exhibited a S : V ratio from 0.3 (*C. curvata*) up to 1.3 (*N. olivacea*).

Maximum growth rate (μ_{max}) was also determined in triplicate for each species, at constant temperature (18°C), under replete nutrients conditions and at nonlimiting light intensity (30 μmoles m^{-2}) under a 14 L : 10 N photoperiod (following recommendations for the Culture Collection of Algae and Protozoa), assessing each culture every two days, and using the exponential growth equation (Pirt 1975):

$$\mu_{max} = \frac{\ln C_2 - \ln C_1}{\Delta t} \quad (5)$$

where C_1 and C_2 are the cell concentrations (cell mL^{-1}) at time $t_1$and t_2, respectively, and Δt is the time interval between t_1 and t_2.

Experimental device and turbulence calibration

Several devices exist to generate controlled turbulent conditions. Oscillating grid and orbital shaker tables are the most widely used systems, although nonhomogeneous turbulence has been reported with the latter (Guadayol et al. 2009). A horizontally oscillating grid system was adopted to generate homogeneous, stationary, and isotropic turbulence similarly to the device used by Schapira et al. (2006). As filamentous species were used in our experiments, such a device avoids any accidental resuspension of filaments stranded in the mesh, unlike vertical grid systems. Turbulence was generated by movement of the grids in three glass chambers constituting three replicates (R1, R2, and R3; Fig. 1). Each chamber with internal length, width and height measuring $0.17 \times 0.17 \times 0.23$ m was filled with 4.9 L of culture medium (height = 0.17 m) and constituted a chemostat where new medium was added continuously (0.015 L h^{-1}) to obtain a dilution rate of 0.07 d^{-1}. This dilution rate was controlled by a peristaltic pump and corresponded to a high enough residence time (approximately 13 d) to allow the development of all six phytoplankton species (the species with the lowest growth rate doubled its population in less than seven days).The grid was a polycarbonate plate with a mesh size of 4×10^{-2} m. It was placed 5×10^{-3} m above the tank, with 0.165 m immersed, corresponding to a solidity equal to 43% (Fig. 1).

Depending on its oscillating velocity, the grid motion produced different turbulence levels that could be quantified by particle imagery velocimetry (PIV) (Al-Homoud and Hondzo 2007). In each tank, the fluid was seeded with particle tracers (silver-coated hollow glass spheres, 10 μm in diameter) that followed the water movement. The successive positions of particles illuminated by a laser sheet in 0.04×0.04 m windows located in the center of the tank, were recorded at 15 Hz for 17 s (256 pairs of images) using a digital camera (Imager pro X2M). The measuring window was fixed and particles displacement was measured and integrated for numerous distances from the grid. Images where the grid was passing in the measuring window were removed for the averaging calculations. The time interval selected between the acquisitions of two images ranged from 4 ms to 10 ms. This lag time was short enough to avoid particles leaving or entering the camera field, but long enough to record particles displacement between two acquisitions. For each pair of images, the mean and root mean square (RMS)

ACCEPTED MANUSCRIPT

velocities of the particles were calculated using LAVISION software and averaged over the 256 pairs of images. Two sets of measurements with different configurations of the laser and camera positions were conducted to obtain *x*, *y*, and *z* components of particle velocities. The mean particle velocities in *x*, *y*, and *z* were null. We then estimated the turbulent kinetic energy (TKE; $m^2 s^{-2}$; Pope 2003):

$$\mathrm{TKE} = \frac{1}{2}[(Vx_{\mathrm{RMS}})^2 + (Vy_{\mathrm{RMS}})^2 + (Vz_{\mathrm{RMS}})^2] \quad (6)$$

From TKE, we calculated the turbulent velocity *u*:

$$u = \sqrt{2\mathrm{TKE}} \quad (7)$$

And for each grid oscillation velocity, we calculated a turbulent dissipation rate (ε):

$$\varepsilon = \frac{Au^3}{1} \quad (8)$$

with *u* the RMS turbulent velocity, *A* a constant assumed to be of order 1 (Tennekes and Lumley 1972) and l the characteristic size of the largest eddy, commonly assumed to be the mesh size in an oscillating grid system (Peters and Redondo 1997). Experiments were conducted at two turbulence intensities, low ($\varepsilon = 7.9 \times 10^{-5} m^2 s^{-3}$) and high ($\varepsilon = 7.8 \times 10^{-3} m^2 s^{-3}$), which are realistic levels when compared to the range of $10^{-6} m^2 s^{-3}$ to $10^{-3} m^2 s^{-3}$ reported for a straight lowland river (Sukhodolov et al. 1998). These turbulence intensities correspond to different values of characteristic length scales:

$$\text{Kolmogorov scale} \quad \eta_k = \sqrt[4]{\frac{\upsilon^3}{\varepsilon}} \quad (9)$$

$$\text{Batchelor scale} \quad \eta_b = \sqrt[4]{\frac{D^2 \cdot \upsilon}{\varepsilon}} \quad (10)$$

where υ is the kinematic viscosity of the fluid $1 \times 10^{-10} m^2 s^{-1}$ and *D* is the molecular diffusion of inorganic nutrients such as nitrate or orthophosphate ($1 \times 10^{-9} m^2 s^{-1}$). As previously stated, the Kolmogorov scale is the scale of the smallest vortices due to turbulence before the dissipation of TKE as heat. The Batchelor scale is the scale of the smallest solute concentration gradient that fluid motion will support in the face of molecular diffusion (Jumars et al. 2009). The two turbulence intensities generated in the experiment corresponded to Kolmogorov scales of 334 μm (LT) and 106 μm (HT) and Batchelor scales of 10.6 μm (LT) and 3.3 μm (HT).

Sampling protocol, community structure, and physicochemical analyses

The phytoplankton species were grown in the same nutrient replete medium, which was a mix of diatom medium, bold-basal medium with threefold nitrogen and vitamins, and Jaworski's medium. Each chamber was seeded with the six species at day 0 (*T*0) and the initial biomass of each one (expressed as biovolume) was estimated from cell counts and measurements. Initial biomasses ranged from 2.4×10^4 μm^3 to 7.8×10^5 μm^3 for each species and were not evenly distributed. This bias was probably due to the larger species for which it was very difficult to get accurate counts. This resulted in a slightly higher biomass at *T*0 in LT than in HT although the LT and HT treatments, despite these differences, did not show any significant differences in community structure at *T*0 (*t*-test, $p > 0.1$). A given turbulence level (LT or HT) was then applied and kept constant for 20 d (end of the experiment $T = 20$). Light sources (white light, OSRAM Luminlux daylight) were located on the side each chamber. The LT experiment was conducted for only nine days in one replicate (R3) due to contamination by an unknown ciliated protozoan, which was not observed in R1 or R2. Nutrient limitation was prevented by the continuous input of nutrients. Each chamber was sampled seven times during the 20 d, four centimeter below the surface at the center of the tank and analyzed for nutrient and phytoplankton species composition and biomass. The total volume was kept constant by adjusting the inflow after each sampling. The bottom of each tank (0.03 m above the bottom) was also sampled at the end of the experiment ($T = 20$). At *T*20, we also measured light intensity at the top (0.04 m below the surface) and bottom (0.03 m above the bottom) of each tank. Filtered samples (Whatman GF/F) were analyzed by colorimetric methods to determine the concentrations of total dissolved nitrogen (TDN) (Barnes and Folkard 1951) and total dissolved phosphorus (TDP) (Murphy and Riley 1962). Unfiltered samples were also taken and analyzed for total nitrogen and total phosphorus by persulfate digestion. All nutrient measurements were performed by automated flow injection analyses (BRAN + LUEBBE, auto-analyser III). Phytoplankton samples were fixed with glutaraldehyde as this preserved the flagella (final concentration 2%) for cell counts and size measurements. Algal counts were performed with an inverted microscope and more than 200 cells per species were counted for each sample (Lund et al. 1958). Cell volumes were calculated by measuring at least 20 individual cells of each species in each sample, following Hillebrand et al. (1999). Potential changes in the size of individual species were also monitored.

Statistical analyses

Temporal differences in phytoplankton community structure between the two modalities were assessed by calculating the Hellinger distance between each pair of samples. The Hellinger distance was chosen because it is not influenced by total biomass differences (Legendre and Legendre 1998). A distance matrix was obtained to which was applied the Ward clustering method to obtain a dendrogram quantifying differences between samples according to their phytoplankton structure. This statistical analysis was performed using the R

ACCEPTED MANUSCRIPT

software (R Development Core Team 2010) and Vegan package (Oksanen et al. 2011). Cells, filaments, and colony size were compared between modalities for each species by applying a Kruskal Wallis test followed by a post hoc Nemenyi test (Legendre and Legendre 1998).

Results

Theoretical and measured sinking velocities

Depending on the three morphological traits measured (size, shape, and density), the four nonmotile species were expected to exhibit different sinking velocities in still water (Table 1). According to the modified Stokes equation, species displaying elongated shapes and the largest size expressed as ESR were expected to sink faster (at least five times faster) than flattened colonies. The measured sinking velocities (V_{sm}) were in accordance with this pattern except for *A. formosa* which sank four times faster than predicted. As a result, the two species displaying the highest measured sinking velocities were *S. pulchellum* (large size, elongated shape, low density) and *A. formosa* (intermediate size, flattened colony, high density).

Surface to volume ratio and growth rate

According to their respective S : V ratios, species were expected to display different μ_{max}: with species showing higher S : V ratios growing more rapidly. The maximum growth rates measured were close to our expectations except for *N. olivacea* which, despite having the highest S : V ratio exhibited one of the lowest μ_{max} ($0.17\,d^{-1}$). On the contrary, the growth rate of *A. formosa* and *A. granulata*, which had similar S : V ratios to *N. olivacea*, attained $0.5\,d^{-1}$ (Table 1).

Nutrient and light conditions during the turbulence experiment

Nutrient concentrations were nonlimiting for phytoplankton growth during the entire experiment because of the constant input of new medium into the chemostats. Under LT, TDN, and TDP concentrations increased, respectively, from 81.4 mg L^{-1} to 101.9 mg L^{-1} and from 53.5 mg L^{-1} to 58.1 mg L^{-1} at the end of the experiment. TDN and TDP followed the same trend during the HT experiment, increasing from 131.1 mg L^{-1} to 148.6 mg L^{-1} and from 53.9 mg L^{-1} to 60.6 mg L^{-1}, respectively. With respect to the growth rates of the selected phytoplankton species, the dilution rate in the chemostat was low enough to allow the establishment of stable populations of each species. At the beginning of both turbulence conditions (LT and HT), the light intensity at 0.04 m below the surface was 30 μmoles $m^{-2}s^{-1}$. At *T*20, whereas the same light intensity was measured (30 μmoles $m^{-2}s^{-1}$) in all replicates (under LT and HT) near the surface, the light intensity near the bottom (0.14 m below surface) under LT was higher (9.8 μmoles $m^{-2}s^{-1}$) than that measured at the bottom under HT (5.8 μmoles $m^{-2}s^{-1}$).

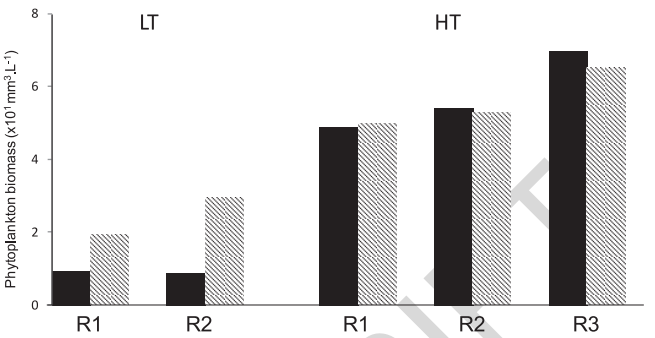

Fig. 2. Total phytoplankton biomass at the end of the experiment (*T*20) in top (full bars) and bottom samples (hatched bars) under LT ($\varepsilon = 7.9 \times 10^{-5}\,m^2\,s^{-3}$) and HT ($\varepsilon = 7.8 \times 10^{-3}\,m^2\,s^{-3}$).

Phytoplankton biomass dynamics

In both experiments, the total phytoplankton biomass increased from *T*0 to *T*20 but differences were apparent between LT and HT (Fig. 2). At *T*20 in both experiments, the phytoplankton biomass was almost six fold higher in HT (57 $mm^3\ L^{-1}$) than in LT (95 $mm^3\ L^{-1}$). This resulted in a lower light intensity reaching the bottom of the tank in HT. The phytoplankton biomass in bottom samples was two or three fold higher (R1 and R2, respectively) than in the surface samples at *T*20 under LT whereas the biomass was similar in top and bottom samples under HT (Fig. 2).

Phytoplankton community structure dynamics

The community structure dynamics from *T*0 to *T*20 differed between LT and HT (Fig. 3). Differences in community structure between LT and HT occurred at *T*3 and persisted until the end of the experiments. Indeed, the hierarchical clusterization based on the Hellinger distance showed that the LT and HT replicates sampled after *T*3 were grouped in distinct clusters. In addition, under HT the bottom samples and surface samples were similar at *T*20 (Hellinger distance < 1), whereas this was not the case under LT. Indeed, one of the highest distances was obtained at *T*20 for the bottom samples and surface samples under LT (Fig. 3).

Under LT, *S. pulchellum* which had the highest sinking velocity ($V_{sm} = 14.4\,\mu m\ s^{-1}$) rapidly disappeared from the water column (Fig. 3). No filaments of this species were observed in the surface samples at *T*9, even though it had accounted for 33% to 50% of the total biomass at the beginning of the experiment. *A. formosa* also sank faster than the other species. Although it was still present in the surface samples, its biomass was two times lower than its initial biomass, representing less than 0.4% of the total biomass at the end of the experiment (compared with 3% to 5% at the beginning) even though it had one of the highest maximum growth rates ($\mu_{max} = 0.42\ d^{-1}$). Although *C. curvata* was

ACCEPTED MANUSCRIPT

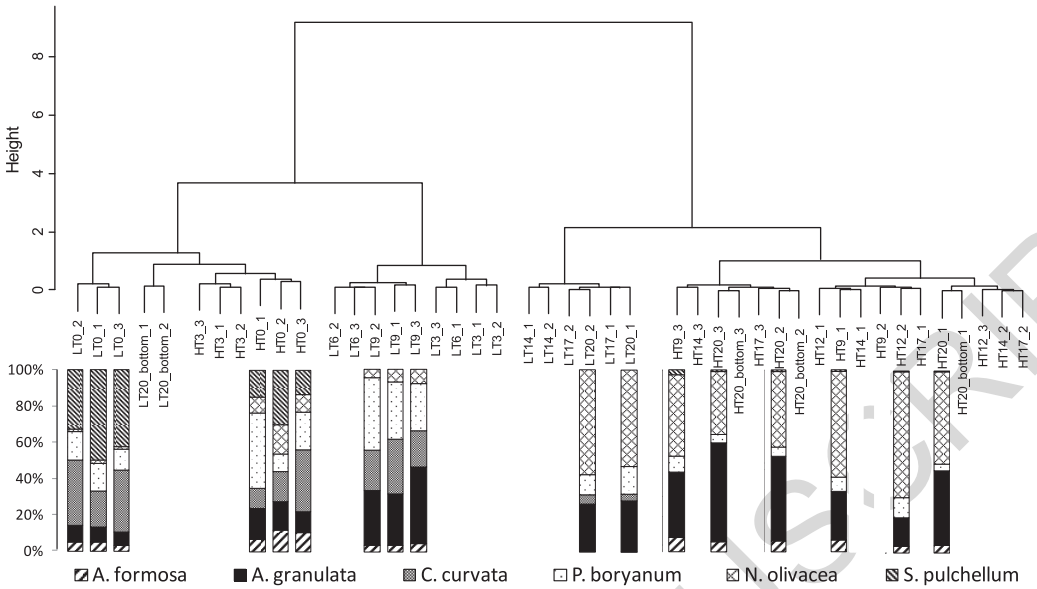

Fig. 3. Hierarchical clustering (Ward method) on the distance matrix (Hellinger distance) of HT and LT replicates based on their species composition, where HT20_2 is the sample of HT, at day 20 from replicate 2. The composition of phytoplankton community (% of biomass) under LT ($\varepsilon = 7.9 \times 10^{-5}\,m^2\,s^{-3}$) and HT ($\varepsilon = 7.8 \times 10^{-3}\,m^2\,s^{-3}$) was also represented for *T*0 = day 0, *T*9 = day 9, and *T*20 = day 20.

flagellated, and therefore, expected to regulate its vertical position, it was one of the rarest species, accounting for less than 5% of the total biomass at the end of the experiment (vs. 30–35% at *T*0).

Sinking species such as *A. granulata* and *P. boryanum*, which had lower sinking velocities, differed in their growth rate ($0.5\,d^{-1}$ and $0.18\,d^{-1}$). They, therefore, accounted for different final proportions of the total biomass, i.e., 25% (8% at *T*0) for the former and 12% (14% at *T*0) for the latter. *N. olivacea*, the small flagellated cell, dominated the community and accounted for more than 50% of the biomass at the end of the experiment vs. 2% at the beginning. Under LT, four of the six species (*A. granulata, C. curvata, N. olivacea*, and *P. boryanum*) increased in biomass.

Under HT, the larger flagellate *C. curvata* completely disappeared three days after *T*0 (Fig. 3). In contrast, even though it accounted for only a small proportion of the total biomass (~ 1% vs. between 14% and 30% at *T*0), *S. pulchellum* was still present in the water column after 3 weeks in all replicates. *A. formosa*, which represented a very small proportion of the total biomass under LT, accounted for 5% of the total biomass under HT at *T*20 (7–14% at *T*0). *P. boryanum* reached a similar level accounting for 4–5% of the total biomass at *T*20. The phytoplankton community was still dominated by *N. olivacea*, but also by *A. granulata* which attained a similar biomass to that of the small flagellate. Both species accounted for nearly 90% of the total phytoplankton biomass at the end of the experiment. Under HT, the biomass of all species (except *C. curvata*) was increased.

Size plasticity

We also investigated whether the different species displayed different values for a given morphofunctional trait under LT and HT. *A. granulata* exhibited variations in filament size between the two turbulence regimes (Fig. 4). Although the filament sizes under the initial conditions were similar, with a mean value of 79 ± 36 μm under LT and 84 ± 37 μm under HT, a significant increase ($p < 0.05$; Nemenyi test) was observed under HT where the mean (151 ± 76 μm) was almost two fold higher than under LT (85 ± 38 μm).

Discussion

Morphology as a proxy for sinking velocity and maximum growth rate

Increasing interest is being shown in the use of morphofunctional traits to explain phytoplankton community structure as these are directly or indirectly related to growth and loss processes. In this study, we attempted to explain phytoplankton community evolution in response to turbulence by focusing on five morphological traits (motility, size, shape, density, and S : V ratio) known to be related to two functional traits (sinking velocity and maximum growth rate).

The first step was to test if these morphological traits accurately reflected the sinking velocity and maximum growth rate and could alone be sufficient to predict these functional traits. Sinking velocity calculations based on the modified Stokes equation (V_{st}) appeared to be in good agreement with the measured values (V_{sm}) for three species (*S. pulchellum, P. boryanum* and *A. granulata*). Interestingly,

ACCEPTED MANUSCRIPT

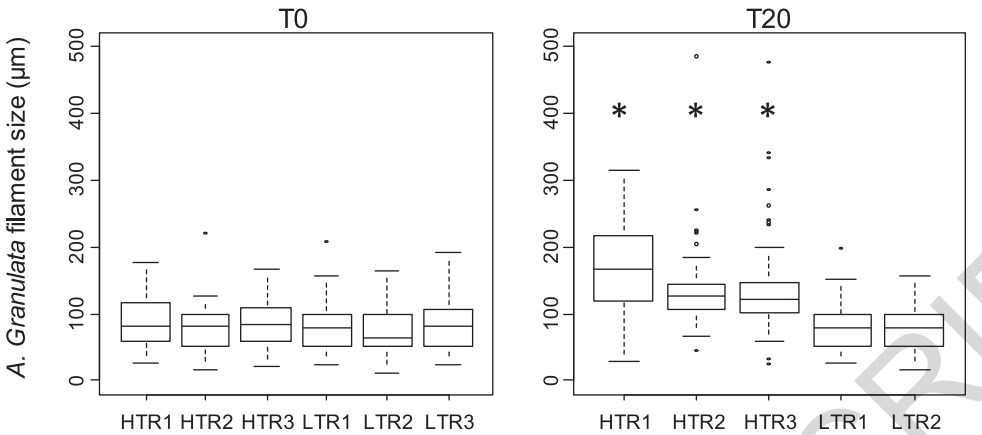

Fig. 4. Filament size of *A. granulata* under HT in three replicates (HTR1, HTR2, HTR3) and under LT (LTR1, LTR2, LTR3) at *T*0 and *T*20. * indicates significant differences ($p < 0.05$; Nemenyi test).

V_{sm} for filaments was closer to the V_{st} calculated for the horizontal position than the V_{st} calculated for the vertical position, thus indicating that filaments are more likely to sink horizontally than sink vertically, which would corroborate the predictions made by Holland (2010). However, some differences emerged for more complex forms like *A. formosa* which sank four times faster than predicted. This deviation from our expectations seemed to arise from the form coefficient value. We used a form coefficient resistance calculated by Padisák et al. (2003) from measurements on large size phytoplankton Polyvinyl chloride (PVC) models sinking in glycerol medium. However, the large form coefficient they found ($\phi = 5$ when colonies contained more than six cells, as in this study) may have been overestimated. Although glycerol was used to increase the viscosity, these authors did not manage to get $Re < 0.1$ for some species (Holland 2010) including *A. formosa* which resulted in an underestimation of sinking velocities and thus an overestimation of form resistance. Based on our results, the form coefficient should be close to 1, reflecting a minor effect of shape on *A. formosa* sinking velocity. Hence, size, shape, and density can be used to predict sinking velocity except for one species. Indeed, although form resistance has been well characterized for cylinders and prolate spheroids (Holland 2010), understanding of more complex shapes is still scanty. Direct observations on modeled phytoplankton, like those conducted by Padisák et al. (2003) should provide significant insights. However, achieving a Reynolds number < 0.1 remains challenging. Smaller particles miming phytoplankton shapes and made with three-dimensional printers could provide a good alternative. This would allow the creation of small, (but large enough to be captured with a camera) accurate complex shapes for which a low Re would be easier to attain.

We also investigated the S : V ratio to predict which species would have the highest maximum growth rate. S : V appeared to provide a good proxy for maximum growth rate, but failed to fully capture the variation between phytoplankton species, especially in the case of diatoms. This limitation had also been highlighted by Edwards et al. (2012) based on a literature analysis of functional traits of 64 marine species. One possible explanation is that diatoms often display vacuoles (Raven and Waite 2004), which reduce the volume of metabolically active material, thereby increasing the effective S/V ratio, and thus the maximum growth rate (Paasche 1960).

Turbulence effect on phytoplankton biomass and community structure

The two levels of turbulence intensity tested induced differences in phytoplankton biomass and community structure. The differences in community structure were independent of the initial biomass. For instance, *S. pulchellum* sustained a steady population under HT although its initial biomass was lower than the initial biomass under LT where the population declined. Under LT, phytoplankton biomass differed between the top (0.04 m below the surface) and bottom of the tank, although it was homogeneous throughout the water column under HT. Furthermore, the community structure in bottom and surface samples was similar under HT (distance < 1, Fig. 3), which would corroborate phytoplankton mixing under HT. Conversely and interestingly, the community structure at the bottom under LT was similar at *T*20 to that of the surface sample at *T*0. As there was no sedimentation constraint at the bottom (which constituted a solid boundary), the community at the bottom did not change over time in comparison to the surface sample where sedimentation occurred.

Although the same species were dominant under LT and HT at *T*20, differences in community structure were observed in response to the degree of turbulence which could be explained by morphofunctional traits. Species of the largest size (*S. pulchellum*) or highest density (*A. formosa*)

ACCEPTED MANUSCRIPT

disappeared from the water column under LT. For some species, the high density was counteracted by the form coefficient resistance (*A. granulata*) which enabled such species to maintain a steady population. As previously stated, *A. formosa* did not fall into this category because its form resistance coefficient had been overestimated. Under LT, the presence of flagella or a flattened shape combined with small size and low density also constituted an advantage by reducing loss through sedimentation. In contrast, and as expected, the fast-sinking species maintained stable populations over time in the water column and attained a higher biomass under HT. This suggests that the highest turbulence level maintained these species in the water column, despite their high intrinsic sinking velocity, which is in accordance with many theoretical (Huisman et al. 1999) and field studies (Bormans and Webster 1999; Peeters et al. 2007; Fraisse et al. 2013).

Besides its effect on vertical distribution, turbulence is also known to act on phytoplankton growth rate, but contrasting effects have been shown (e.g., Berdalet et al. 2007) and no clear pattern has been put forward. Negative effects of turbulence on dinoflagellates have been well documented (Berdalet 1992; Sullivan and Swift 2003) even if such effects also occur across taxa, affecting Chlorophyta (Hondzo and Lyn 1999), Cyanobacteria (Regel et al. 2004) Cyanobacteria and Diatoms (Wang et al. 2012). In our case, a negative effect was observed on the large flagellated species *C. curvata* (Cryptophyceae). However, our microscopic observations did not suggest that any mechanical destruction had occurred, such as flagella loss, which had been reported by Thomas and Gibson (1990) on dinoflagellates. This indicates that turbulence can negatively affect phytoplankton in several ways and few are well-understood.

Turbulence could also have a positive effect on growth rate, depending on cell size, by increasing the nutrient concentrations in the vicinity of the cell (Karp-Boss et al. 1996; Peters et al. 2006). Indeed, growth rate depends on two phenomena: nutrient delivery to the cell (Q) and transport across the membrane (V). Turbulence leads to an increased growth rate by increasing Q. However, when nutrients are nonlimiting, Q overcomes V so that V becomes the process limiting nutrient uptake (Karp-Boss et al. 1996), which was the case in this study. Nevertheless, even if the underlying mechanisms have not yet been identified, increases in phytoplankton growth rate have already been reported under replete nutrient conditions, in response to increased turbulence (Iversen et al. 2009; Wang et al. 2012). The small flagellated species *N. olivacea* was dominant under both turbulence levels in our experiment and displayed a much higher growth rate under HT than under LT and under LT than in still water. The hypothesis of an increase in nutrient fluxes toward the cell, due to the laminar flow induced by turbulence, does not hold as the nutrient concentrations were never limiting. *N. olivacea* is a flagellated cell smaller than the Batchelor scale (at least under LT) and it could be that it forages patches of higher nutrient concentrations. But once again, this hypothesis does not hold as it grew under replete nutrient conditions. The observed growth rate enhancement might be due to the different light intensities experienced by *N. olivaecea* (Litchman 2000) resulting from its movement through the water column by turbulent diffusion. The slightly higher light gradient under HT (surface: 35 μmoles $m^{-2}s^{-1}$; bottom: 5.8 μmoles $m^{-2}s^{-1}$) than under LT (surface: 35 μmoles $m^{-2}s^{-1}$; bottom: 9.8 μmoles $m^{-2}s^{-1}$) could explain the difference in growth rates between the two modalities.

In this experiment, to dominate the phytoplankton community, a species had to display morphofunctional traits related to a low sinking velocity under LT, or a high growth rate under HT. One surprising result was that the same two species dominated the community under both conditions. It was not unexpected that *N. olivacea*, which possesses flagella and exhibited the highest growth rate, dominated the community under both turbulence levels. *A. granulata* also displayed a high growth rate compared to the other species which would explain its dominance under HT. However, its codominance with *N. olivacea* under LT (even if less marked) was unexpected as its morphofunctional traits, as compared to those of the other species, were related to a high sinking velocity. The reason could be linked to the smaller size of the filament under LT than under HT.

Turbulence and morphological plasticity

Indeed, during the experiment, the *A. granulata* filament doubled its initial size 9 d after the beginning of HT whereas the cell size remained similar. This result is surprising as it was expected that the filament size under HT would be smaller than under LT. Indeed, the lower Kolomogorov scale (defining a lower eddy motion) produced under HT was expected to result in mechanical destruction, (Thomas and Gibson 1990) and therefore, in a smaller filament size. A similar increase in filament size in response to an increased turbulence level has already reported (Arin et al. 2002), but no explanation has been proposed. Our results suggest that it could be linked to the sedimentation resistance. Indeed, according to the Stokes equation, the sinking velocity should increase as the filament size increases. *A. granulata* would attain a greater size under HT as the higher turbulent diffusion would be able to keep the longer filaments in suspension. This suggests a potential trait adjustment resulting in an increase in fitness of this species.

The interaction of filamentous species with turbulent flow is a complex phenomenon. Indeed, the motion of a chain is dependent on its flexibility and orientation (Musielak et al. 2009) and differences in flexibility occur between filamentous diatom species and are related to the connection between cells (Young et al. 2012). This feature requires more

ACCEPTED MANUSCRIPT

specific investigation to understand the evolution of sinking velocity in different turbulent intensities.

Extrapolation to natural systems

By applying the turbulence levels characteristic of lotic systems (Sukhodolov et al. 1998), we were able to show how turbulence shaped the community in terms of morphofunctional traits. However, caution is required when extrapolating these results to natural systems, especially deep stratified systems with a turbulent surface mixed layer overlying a less turbulent bottom layer. Indeed in these cases, phytoplankton leaving the base of the surface mixing layer cannot be resuspended (O'Brien et al. 2003). As our device consisted of small tanks with a solid bottom, potential resuspension from the bottom upward under HT cannot be excluded, even if the mean vertical velocity of water was null (measured through PIV under LT and HT). Resuspension was less likely to occur under LT, as the biomass of all species was greater at the bottom of the tank. Hence, although our results cannot be transferred stricto sensu to natural systems, certain analogies can be put forward. Indeed, the HT condition reflected shallow systems where light is not limited even at the bottom, where turbulence is high and where the phytoplankton community can be influenced by resuspension, as is the case for some rivers (Fraisse et al. 2013). In contrast, the LT condition is representative of deeper systems where reduced mixing leads to the dominance of species displaying low sinking velocities (Winder et al. 2009).

Furthermore, it should be kept in mind when extending these results to ecosystems like lakes or oceans, that the turbulence levels used in this study were rather high and characteristic of rivers. Turbulence levels in lentic or marine systems are generally even lower than the lowest condition used in our study (i.e., $7.9 \times 10^{-5}\,m^2\,s^{-3}$) with $10^{-8}\,m^2\,s^{-3}$ to $10^{-6}\,m^2\,s^{-3}$ as typical values for the upper mixed layer in oceans (Guadayol and Peters 2006) and with $10^{-11}\,m^2\,s^{-3}$ to $10^{-5}\,m^2\,s^{-3}$ in lakes (Hondzo and Warnaars 2008). Hence, lentic and marine species should to exhibit morphofunctional traits related to lower sinking velocities, which is generally the case as marine phytoplankton are usually small or display cytoplasmic extensions that increase their form coefficient resistance. Furthermore, it has been stated that turbulence changes could explain the observed phytoplankton succession between diatoms and dinoflagellates based on their morphofunctional traits in coastal ecosystems (Margalef 1978). Our study corroborates these results and one of the principal assumptions that turbulence is a major force shaping phytoplankton cells through evolution.

References

Aksnes, D. L., and J. K. Egge. 1991. A theoretical model for nutrient uptake in phytoplankton. Mar. Ecol. Prog. Ser. **70**: 65–72. doi:10.3354/meps070065

Al-Homoud, A., and M. Hondzo. 2007. Energy dissipation estimates in oscillating grid setup: LDV and PIV measurements. Environ. Fluid Mech. **7**: 143–158. doi:10.1007/s10652-007-9020-0

Arin, L., C. Marrasé, M. Maar, F. Peters, M. Sala, and M. Alcaraz. 2002. Combined effects of nutrients and small-scale turbulence in a microcosm experiment. I. Dynamics and size distribution of osmotrophic plankton. Aquat. Microb. Ecol. **29**: 51–61. doi:10.3354/ame029051

Banse, K. 1976. Rates of growth, respiration and photosynthesis of unicellular algae as related to cell size: A review. J. Phycol. **12**: 135–140. doi:10.1111/j.1529-8817.1976.tb00490.x

Barnes, H., and A. R. Folkard. 1951. The determination of nitrite. Analyst **76**: 599–603. doi:10.1039/an9517600599

Berdalet, E. 1992. Effects of turbulence on the marine dinoflagellate *Gymnodinium nelsonii*. J. Phycol. **28**: 267–272. doi:10.1111/j.0022-3646.1992.00267.x

Berdalet, E., F. Peters, V. L. Koumandou, C. Roldán, Ò. Guadayol, and M. Estrada. 2007. Species-specific physiological response of dinoflagellates to quantified small-scale turbulence. J. Phycol. **43**: 965–977. doi:10.1111/j.1529-8817.2007.00392.x

Bormans, M., and S. A. Condie. 1998. Modelling the distribution of *Anabaena* and *Melosira* in a stratified river weir pool. Hydrobiologia **364**: 3–13. doi:10.1023/A:1003103706305

Bormans, M., and I. T. Webster. 1999. Modelling the spatial and temporal variability of diatoms in the River Murray. J. Plankton Res. **21**: 581–598. doi:10.1093/plankt/21.3.581

Clift, R., J. R. Grace, and M. E. Weber. 1978. Bubbles, Drops, and Particles. Academic press incorporation. doi:10.3989/scimar.2005.69n2187

Descy, J.-P., and V. Gosselain. 1994. Development and ecological importance of phytoplankton in a large lowland river (River Meuse, Belgium). Hydrobiologia **289**: 139–155. doi:10.1007/BF00007415

Edwards, K. F., M. K. Thomas, C. A. Klausmeier, and E. Litchman. 2012. Allometric scaling and taxonomic variation in nutrient utilization traits and maximum growth rate of phytoplankton. Limnol. Oceanogr. **57**: 554–566. doi:10.4319/lo.2012.57.2.0554

Estrada, M., and E. Berdalet. 1997. Phytoplankton in a turbulent world. Sci. Mar. **61**: 125–140.

Fraisse, S., M. Bormans, and Y. Lagadeuc. 2013. Morpho-functional traits reflect differences in phytoplankton community between rivers of contrasted flow regime. Aquat. Ecol. **47**: 315–327. doi:10.1007/s10452-013-9446-z

Gervais, F. 1997. Diel vertical migration of *Cryptomonas* and *Chromatium* in the deep chlorophyll maximum of a eutrophic lake. J. Plankton Res. **19**: 533–550. doi:10.1093/plankt/19.5.533

Guadayol, O., C. Marrasé, F. Peters, E. Berdalet, C. Roldan, and A. Sabata. 2009. Responses of coastal osmotrophic

ACCEPTED MANUSCRIPT

planktonic communities to simulated events of turbulence and nutrient load throughout a year. J. Plankton Res. **31**: 583–600. doi:10.1093/plankt/fbp019

Guadayol, O., and F. Peters. 2006. Analysis of wind events in a coastal area: A tool for assessing turbulence variability for studies on plankton. Sci. Mar. **70**: 9–20.

Hillebrand, H., C. D. Dürselen, D. Kirschtel, U. Pollingher, and T. Zohary. 1999. Biovolume calculation for pelagic and benthic microalgae. J. Phycol. **35**: 403–424. doi:10.1046/j.1529-8817.1999.3520403.x

Holland, D. P. 2010. Sinking rates of phytoplankton filaments oriented at different angles: Theory and physical models. J. Plankton Res. **32**: 1327–1326. doi:10.1093/plankt/fbq044

Hondzo, M., and D. Lyn. 1999. Quantified small-scale turbulence inhibits the growth of a green alga. Freshw. Biol. **41**: 51–61. doi:10.1046/j.1365-2427.1999.00389.x

Hondzo, M., and T. A. Warnaars. 2008. Coupled effects of small-scale turbulence and phytoplankton biomass in a small stratified lake. J. Environ. Eng. **134**: 954–961. doi:10.1061/(ASCE)0733-9372(2008)134:12(954)

Hötzel, G., and R. Croome. 1999. A phytoplankton manual for Australian freshwaters. Land and Water Ressource Research and Development Corporation. Camberra Act 2605.

Huisman, J., P. van Oostveen, and F. J. Weissing. 1999. Critical depth and critical turbulence: Two different mechanisms for the development of phytoplankton blooms. Limnol. Oceanogr. **44**: 1781–1787. doi:10.4319/lo.1999.44.7.1781

Iversen, K. R., and others. 2009. Effects of small-scale turbulence on lower trophic levels under different nutrient conditions. J. Plankton Res. **32**: 197–208. doi:10.1093/plankt/fbp113

Jaworski, G. H. M., S. W. Wiseman, and C. S. Reynolds. 1988. Variability in sinking rate of the freshwater diatom *Asterionella formosa*: The influence of colony morphology. Br. Phycol. J. **23**: 167–176. doi:10.1080/00071618800650201

Jumars, P. A., J. H. Trowbridge, E. Boss, and L. Karp-Boss. 2009. Turbulence plankton interactions: A new cartoon. Mar. Ecol. **30**: 133–150. doi:10.1111/j.1439-0485.2009.00288.x

Karp-Boss, L., E. Boss, and P. A. Jumars. 1996. Nutrient fluxes to planktonic osmotrophs in the presence of fluid motion. Oceanogr. Mar. Biol. Annu. Rev. **34**: 71–107.

Kiøboe, T. 1993. Turbulence, phytoplankton cell size, and the structure of pelagic food webs. Adv. Mar. Biol. **29**: 1–72. doi:10.1016/S0065-2881(08)60129-7

Kruk, C., E.T.H.M. Peeters, E. H. Van Nes, V. L. M. Huszar, L. S. Costa, and M. Scheffer. 2011. Phytoplankton community composition can be predicted best in terms of morphological groups. Limnol. Oceanogr. **56**: 110–118. doi:10.4319/lo.2011.56.1.0110

Kruk, C., and others. 2010. A morphological classification capturing functional variation in phytoplankton. Freshw. Biol. **55**: 614–627. doi:10.1111/j.1365-2427.2009.02298.x

Lagadeuc, Y. 2005. Nutrient fluxes toward phytoplankton: Is it useful to consider turbulence intermittency? Acta Biotheor. **53**: 371–379. doi:10.1007/s10441-005-4891-2

Lazier, J. R. N., and K. H. Mann. 1989. Turbulence and the diffusive layers around small organisms. Deep Sea Res. **36**: 1721–1733. doi:10.1016/0198-0149(89)90068-X

Legendre, L., and P. Legendre. 1998. Numerical Ecology, 2nd ed. Elsevier Science.

Litchman, E. 2000. Growth rates of phytoplankton under fluctuating light. Freshw. Biol. **44**: 223–235. doi:10.1046/j.1365-2427.2000.00559.x

Litchman, E., and C. A. Klausmeier. 2008. Trait-based community ecology of phytoplankton. Annu. Rev. Ecol. Evol. Syst. **39**: 615–639. doi:10.1146/annurev.ecolsys.39.110707.173549

Lund, J. W. G., C. Kipling, and E. D. Le Cren. 1958. The inverted microscope method of estimating algal numbers and the statistical basis of estimations by counting. Hydrobiologia **11**: 143–170. doi:10.1007/BF00007865

Marañón, E., and others. 2013. Unimodal size scaling of phytoplankton growth and the size dependence of nutrient uptake and use. Ecol. Lett. **16**: 371–379. doi:10.1111/ele.12052][23279624

Margalef, R. 1978. Life-forms of phytoplankton as survival alternatives in an unstable environment. Oceanol. Acta **1**: 493–509.

McGill, B., B. Enquist, and E. Weiher. 2006. Rebuilding community ecology from functional traits. Trends Ecol. Evol. **21**: 178–185. doi: 10.1016/j.tree.2006.02.002

McNown, J., and J. Malaika. 1950. Effects of particle shape on settling velocity at low reynolds numbers. Trans Am Geophys. Union **31**: 74–81. doi:10.1029/TR031i001p00074

Murphy, J., and J. P. Riley. 1962. A modified simple solution method for the determination of phosphate in natural waters. Anal. Chim. Acta **27**: 31–36. doi:10.1016/S0003-2670(00)88444-5

Musielak, M. M., L. Karp-Boss, P. A. Jumars, and L. J. Fauci. 2009. Nutrient transport and acquisition by diatom chains in a moving fluid. J. Fluid Mech. **638**: 401–421. doi:10.1017/S0022112009991108

Naselli-Flores, L., and R. Barone. 2011. Fight on plankton! Or, phytoplankton shape and size as adaptive tools to get ahead in the struggle for life. Cryptogam. Cryptogamie Algol. **32**: 157–204. doi:10.7872/crya.v32.iss2.2011.157

O'Brien, K. O., G. N. Ivey, D. P. Hamilton, A. M. Waite, P. M. Visser. 2003. Simple mixing criteria for the growth of negatively buoyant phytoplankton. Limnol. Oceanogr. **48**: 1326–1327. doi:10.4319/lo.2003.48.3.1326

Oksanen, J., and others. 2011. Vegan: community ecology package.

ACCEPTED MANUSCRIPT

Paasche, E. 1960. On the relationship between primary production and standing stock of phytoplankton. J. Cons. Perm. Int. Explor. Mer. **26**: 33–48. doi:10.1093/icesjms/26.1.33

Padisák, J., E. Soróczki-Pintér, and Z. Rezner. 2003. Sinking properties of some phytoplankton shapes and the relation of form resistance to morphological diversity of plankton: An experimental study. Hydrobiologia **500**: 243–257. doi:10.1023/A:1024613001147

Pahlow, M., U. Riesbell, and D. A. Wolf-Gladrow. 1997. Impact of cell shape and chain formation on nutrient acquisition by marine diatoms. Limnol. Oceanogr. **42**: 1660–1672. doi:10.4319/lo.1997.42.8.1660

Peeters, F., D. Straile, A. Lorke, and D. Ollinger. 2007. Turbulent mixing and phytoplankton spring bloom development in a deep lake. Limnol. Oceanogr. **52**: 286–298. doi:10.4319/lo.2007.52.1.0286

Peters, F., L. Arin, C. Marrasé, E. Berdalet, and M. M. Sala. 2006. Effects of small-scale turbulence on the growth of two diatoms of different size in a phosphorus-limited medium. J. Mar. Syst. **61**: 134–148. doi:10.1016/j.jmarsys.2005.11.012

Peters, F., and J. M. Redondo. 1997. Turbulence generation and measurement: Application to studies on plankton. Sci. Mar. **61**: 205–228.

Pirt, S. J. 1975. Principles of microbe and cell cultivation, Wiley-Blackwell.

Pithart, D. 1997. Diurnal vertical migration study during a winter bloom of cryptophyceae in a foodplain pool. Int. Rev. Gesamten Hydrobiol. **82**: 33–46. doi:10.1002/iroh.19970820106

Pope, S. B. 2003. Turbulent flows. Cambridge Univ. Press.

R Development Core Team. 2010. R: A language and environment for statistical computing. R Foundation for Statistical Computing, Vienna, Austria. ISBN 3-900051-07-0. Available from: http://www.R-project.org.

Raven, J. A., and A. M. Waite. 2004. The evolution of silicification in diatoms: Inescapable sinking and sinking as escape? New Phytol. **162**: 45–61. doi:10.1111/j.1469-8137.2004.01022.x

Regel, R. H., J. D. Brookes, G. G. Ganf, and R. W. Griffiths. 2004. The influence of experimentally generated turbulence on the Mash01 unicellular *Microcystis aeruginosa* strain. Hydrobiologia **517**: 107–120. doi:10.1023/B:HYDR.0000027341.08433.32

Reynolds, C. S. 2000. Hydroecology of river plankton: The role of variability in channel flow. Hydrol. Process. **14**: 3119–3132. doi:10.1002/1099-1085(200011/12)14:16/17<3119::AID-HYP137>3.0.CO;2-6

Reynolds, C. S. 2006. Ecology of phytoplankton. Cambridge Univ. Press.

Reynolds, C. S. 2007. Variability in the provision and function of mucilage in phytoplankton: Facultative responses to the environment. Hydrobiologia **578**: 37–45. doi:10.1007/s10750-006-0431-6

Schapira, M., L. Seuront, and V. Gentilhomme. 2006. Effects of small-scale turbulence on *Phaeocystis globosa* (Prymnesiophyceae) growth and life cycle. J. Exp. Mar. Biol. Ecol. **335**: 27–38. doi:10.1016/j.jembe.2006.02.018

Smayda, T. J., and C. S. Reynolds. 2001. Community assembly in marine phytoplankton: Application of recent models to harmful dinoflagellate blooms. J. Plankton Res. **23**: 447–461. doi:10.1093/plankt/23.5.447

Smith, I. R. 1982. A simple theory of algal deposition. Freshw. Biol. **12**: 445–449. doi:10.1111/j.1365-2427.1982.tb00639.x

Sukhodolov, A., M. Thiele, and H. Bungartz. 1998. Turbulence structure in a river reach with sand bed. Water Resour. Res. **34**: 1317–1334. doi:10.1029/98WR00269

Sullivan, J. M., and E. Swift. 2003. Effects of small-scale turbulence on net growth rate and size species of marine dinoflagellates. J. Phycol. **94**: 83–94. doi:10.1046/j.1529-8817.2003.02094.x

Tavernini, S., E. Pierobon, and P. Viaroli. 2011. Physical factors and dissolved reactive silica affect phytoplankton community structure and dynamics in a lowland eutrophic river (Po river, Italy). Hydrobiologia **669**: 213–225. doi:10.1007/s10750-011-0688-2

Tennekes, H. H., and J. L. Lumley. 1972. In A first course in turbulence, M. Press [ed.]. MIT Press.

Thomas, W. H., and C. H. Gibson. 1990. Effects of small-scale turbulence on microalgae. J. Appl. Phycol. **2**: 71–77. doi:10.1007/BF02179771

Thorpe, S. A. 2007. An introduction to ocean turbulence, Cambridge Univ. Press.

Violle, C., M.-L. Navas, D. Vile, E. Kazakou, C. Fortunel, I. Hummel, and E. Garnier. 2007. Let the concept of trait be functional! Oikos **116**: 882–892. doi: 10.1111/j.2007.0030-1299.15559.x

Walsby, A. E. 1994. Gas vesicles. Microbiol. Rev. **58**: 94–144.

Walsby, A. E., and D. P. Holland. 2006. Sinking velocities of phytoplankton measured on a stable density gradient by laser scanning. J. R. Soc. Interface **3**: 429–439. doi:10.1098/rsif.2005.0106

Wang, P., H. Shen, and P. Xie. 2012. Can hydrodynamics change phosphorus strategies of diatoms? Nutrient levels and diatom blooms in lotic and lentic ecosystems. Microb. Ecol. **63**: 369–382. doi:10.1007/s00248-011-9917-5

Weithoff, G. 2003. The concepts of "plant functional types" and "functional diversity" in lake phytoplankton: A new understanding of phytoplankton ecology? Freshw. Biol. **48**: 1669–1675. doi:10.1046/j.1365-2427.2003.01116.x

Winder, M., J. E. Reuter, and S. G. Schladow. 2009. Lake warming favours small-sized planktonic diatom species. Proc. R. Soc. B **276**: 427–435. doi:10.1098/rspb.2008.1200

Young, A. M., L. Karp-Boss, P. A. Jumars, and E. N. Landis. 2012. Quantifying diatom aspirations: Mechanical properties of chain-forming species. Limnol. Oceanogr. **57**: 1789–1801. doi:10.4319/lo.2012.57.6.1789

ACCEPTED MANUSCRIPT

Acknowledgments

We thank Alain Faisan and Alexandre Valence (Physic Institute of Rennes) for their precious help in design and construction of the experimental device (turbulence generator coupled with a chemostat) and its turbulence calibration by PIV. We also thank Mélanie Racine who performed algal density measurements. We wish to acknowledge Frances Pick (University of Ottawa) and Elisa Berdalet (Institute of Marine Sciences, Barcelona) for their relevant scientific comments and Nicolas Fraisse for its contribution to the figure 1. We also thank Diana Warwick and Frances Pick for English language revision. Finally, we are grateful to the associate editor John A. Raven and four anonymous reviewers whose comments and suggestions substantially improve the manuscript. This work was supported by a grant from the CNRS and Veolia Environment to Stéphane Fraisse.

Submitted 30 June 2014
Revised 21 January 2014
Accepted 12 January 2015

Associate editor: John Albert Raven

ACCEPTED MANUSCRIPT